Multiscale Strain as a Predictor of Impact-Induced Fissuring in Articular Cartilage

Corinne R. Henak[1]
Meinig School of Biomedical Engineering,
Cornell University,
Ithaca, NY 14853

Lena R. Bartell
Department of Applied and Engineering Physics,
Cornell University,
Ithaca, NY 14853

Itai Cohen
Department of Physics,
Cornell University,
Ithaca, NY 14853

Lawrence J. Bonassar[2]
Meinig School of Biomedical Engineering,
149 Weill Hall,
Cornell University,
Ithaca, NY 14853;
Sibley School of Mechanical
and Aerospace Engineering,
Cornell University,
Ithaca, NY 14853
e-mail: LB244@cornell.edu

Mechanical damage is central to both initiation and progression of osteoarthritis (OA). However, specific causal links between mechanics and cartilage damage are incompletely understood, which results in an inability to predict failure. The lack of understanding is primarily due to the difficulty in simultaneously resolving the high rates and small length scales relevant to the problem and in correlating such measurements to the resulting fissures. This study leveraged microscopy and high-speed imaging to resolve mechanics on the previously unexamined time and length scales of interest in cartilage damage, and used those mechanics to develop predictive models. The specific objectives of this study were to: first, quantify bulk and local mechanics during impact-induced fissuring; second, develop predictive models of fissuring based on bulk mechanics and local strain; and third, evaluate the accuracy of these models in predicting fissures. To achieve these three objectives, bovine tibial cartilage was impacted using a custom spring-loaded device mounted on an inverted microscope. The occurrence of fissures was modulated by varying impact energy. For the first objective, during impact, deformation was captured at 10,000 frames per second and bulk and local mechanics were analyzed. For the second objective, data from samples impacted with a 1.2 mm diameter rod were fit to logistic regression functions, creating models of fissure probability based on bulk and local mechanics. Finally, for the third objective, data from samples impacted with a 0.8 mm diameter rod were used to test the accuracy of model predictions. This study provides a direct comparison between bulk and local mechanical thresholds for the prediction of fissures in cartilage samples, and demonstrates that local mechanics provide more accurate predictions of local failure than bulk mechanics provide. Bulk mechanics were accurate predictors of fissure for the entire sample cohort, but poor predictors of fissure for individual samples. Local strain fields were highly heterogeneous and significant differences were determined between fissured and intact samples, indicating the presence of damage thresholds. In particular, first principal strain rate and maximum shear strain were the best predictors of local failure, as determined by concordance statistics. These data provide an important step in establishing causal links between local mechanics and cartilage damage; ultimately, data such as these can be used to link macro- and micro-scale mechanics and thereby predict mechanically mediated disease on a subject-specific basis.
[DOI: 10.1115/1.4034994]

Introduction

While it is known that osteoarthritis (OA) develops as a result of mechanical loading, specific causal links between mechanics and cartilage damage are incompletely understood. Because it can be triggered by a single mechanical event, post-traumatic OA (PTOA) provides a well-defined lens through which to determine mechanical causes of cartilage damage. PTOA causes structural damage and chondrocyte injury, among other changes [1,2]. Rapid impact injury, an ex vivo model of cartilage damage, can create fissures that extend approximately 100–300 μm from the articular surface [3,4]. Such fissures are thought to predispose cartilage and chondrocytes to further damage in the pathway to PTOA. Thus, rapid impact injury provides a scenario through which causal links between mechanics and OA can be studied.

Linking mechanics and cartilage damage using impact injury requires experimental measurements over short time scales and small length scales. Specifically, impact injuries of the type that cause PTOA only last a few milliseconds [5]. Additionally, impact injury causes spatially heterogeneous strain fields, which are further confounded by spatial heterogeneity in cartilage material properties. Cartilage stiffness varies by up to an order of magnitude through the depth, with a compliant layer in the most superficial 100–300 μm [6–10]. Thus, local strain fields, with resolution at or below 100 μm, are necessary to capture length scales pertinent to both fissures and material heterogeneity in cartilage.

Due to technical challenges, most previous research has focused on bulk mechanics, wherein values are averaged over the entire 1–3 mm cartilage thickness (e.g., Refs. [11–30]). Results from such measurements, however, often propose inexact thresholds based on limited groups of mechanical parameters, preventing the extraction of specific thresholds (e.g., Refs. [12,20,22], and [31–35]). When such thresholds are reported, they are often inconsistent between studies. For example, one set of studies showed fissures at impact energies as low as 1 J [22,23], while another study did not report fissures at that energy level [33]. In terms of peak stress, fissures have been reported in samples loaded to ~15–30 MPa in some studies [13,16], with other studies not reporting fissures in the same stress range [12,34]. Moreover, when thresholds have been proposed, they are seldom validated. For example, a 5.45 MPa shear stress threshold has been proposed for 50% probability of fissure by fitting experimental data [36], but its predictive ability has not been tested. Therefore, to address these challenges, the objectives of this study were three-fold: first, to quantify bulk mechanics and local strains during impact-induced fissuring; second, to develop predictive models of fissuring based on bulk mechanics and local strain; and third, to

---

[1]Present address: Department of Mechanical Engineering, University of Wisconsin-Madison, Madison, WI 53706.

[2]Corresponding author.

evaluate the accuracy of those models in predicting fissures in a second set of samples using a distinct impact geometry.

Methods

Sample Preparation. Articular cartilage was dissected from immature bovine stifle joints (nine animals, 1–3 days old, sex unknown and assumed random; Gold Medal Packing, Oriskany, NY). Cylindrical cartilage explants were removed from the peripheral medial and lateral tibial plateau using a 6 mm diameter biopsy punch and scalpel. This location was selected due to its lack of preferred collagen orientation at the articular surface [6]. Samples were stored at −20 °C between dissection and testing.

For testing, cylinders were cut in half to make hemicylinders and trimmed to approximately 1 mm thick, creating impact samples; a total of 35 hemicylindrical samples were impacted. Samples were trimmed to provide consistent bulk behavior, with 1 mm thickness selected to be able to view both the impact tip and the backplate during impact. Two staining protocols were used, one to visualize fissures and one to visualize cartilage deformations during impact. To visualize cartilage structure and determine the presence of fissures, samples were stained in 28 μM 5-dichlorotriazinylaminofluorescein (DTAF) (Invitrogen, Waltham, MA) for 30–120 min. Five-DTAF is a general-purpose amine-reactive dye that stains the entire cartilage matrix, thus enabling matrix structure and integrity to be viewed via fluorescence microscopy. Following staining in 5-DTAF, samples were rinsed briefly in phosphate-buffered saline (PBS) to remove any unbound dye. Next, to create visual texture for the evaluation of local deformations, approximately 1 μl of polystyrene microspheres (2 μm carboxylate particles in 2.5% aqueous solution; Polysciences, Inc., Warrington, PA) were placed on the cut surface of the cylinder and the spheres were allowed to adhere to the sample for 10 min at room temperature and humidity. Samples were then attached to the impact device backplate using cyanoacrylate [37] and rehydrated in PBS for at least 10 min prior to impact. Pilot studies confirmed that this staining protocol had no effect on sample wet weight or depth-dependent shear properties following rehydration.

Impact Injury. Cartilage samples were impacted using a custom spring-loaded device [37] (Fig. 1(a)). A cylindrical impact rod, oriented longitudinally, contacted the articular surface of cartilage samples submerged in PBS. Impact energy was controlled by varying the amount of spring compression, which set an upper bound on the energy. During impact, samples were mounted to a backplate that acted as a cantilevered spring. The backplate's deformation was calibrated and then imaged during impact to measure the time-dependent impact force [37]. The impact device was mounted on an inverted confocal microscope (LSM 5 LIVE, Carl Zeiss, Inc., Jena, Germany). During impact, high-speed images of sample deformation and backplate deformation were captured using a camera (v7.1, Vision Research, Wayne, NJ) and a mercury arc lamp (HBO 100, Carl Zeiss, Inc., Jena, Germany) transmitted through the microscope in epifluorescence mode. Images were captured at 10,000 frames per second using a 5× objective, resulting in a spatial resolution of 4.5 μm per pixel. Before and after impact, samples were imaged in confocal mode to visualize the matrix integrity. A range of spring impact energies were used (0.43–0.56 J) such that some samples fissured and others remained intact. Each sample was impacted only once, using high-speed images to extract strains and force. Over all samples, the average time to maximum indentation was 1.83 ± 0.63 ms, with samples in the impact test fixture for approximately 10 min per test.

Two rods of different diameters were used to create distinct loading scenarios. Twenty-three hemicylindrical samples were impacted with a 1.2 mm diameter rod. These data were used to quantify bulk and local mechanics, and to develop predictive models. A second series of 12 samples were impacted with a 0.8 mm diameter rod and these data were used to test how well the models predicted failure. All samples were categorized as either intact or fissured, using confocal images captured with 5× and 10× objectives. The two rods created distinct fissure geometries (Figs. 1(b) and 1(c)). The 1.2 mm diameter rod created longer fissures with smaller open areas compared to the 0.8 mm diameter rod. These differences between fissures created by the two rods underscored their ability to create distinct local strain fields, and thus test the predictive models.

Bulk Strain and Force. Bulk compressive strain, strain rate, force, and force rate were calculated under the impact rod for 11 samples. Articular surface displacement (d_{AS}) and backplate displacement (d_B) were determined using custom code with intensity-based image registration in MATLAB (Mathworks, Natick, MA). The undeformed sample depth (L_0) was manually measured using the reference image taken prior to impact. Bulk compressive strain during impact ($\varepsilon(t)$) was calculated as a function of time using the following equation:

$$\varepsilon(t) = \frac{L_0 + (d_B(t) - d_{AS}(t))}{L_0} \qquad (1)$$

Bulk force during impact ($F(t)$) was calculated using Eq. (2) via a predetermined force–displacement backplate calibration constant (k) [37]
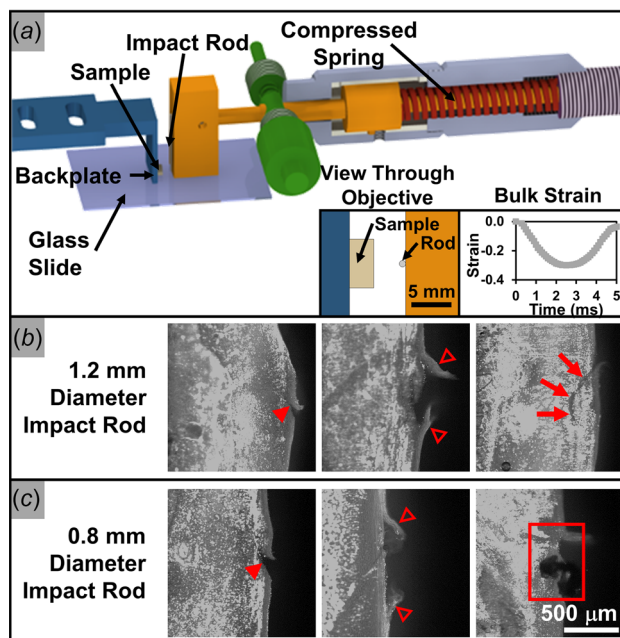

Fig. 1 Impact device and resulting fissures. Impact was applied via a custom spring-loaded impact device, which sat on an inverted microscope (a). The amount of spring compression controlled the upper bound on the impact energy and the microscope could be used either in epifluorescence mode with a high-speed camera or in confocal mode. Images taken during impact were used to calculate force from the backplate deflection, and to calculate strain ((a), inset). To produce a wide array of fissures, two different diameter rods were used: 1.2 mm diameter (b) and 0.8 mm diameter (c). Rods were oriented longitudinally such that a circular impact was visible through the objective and the impact geometry was as consistent as possible along the third dimension (optical axis). Both rods created some small angular fissures (filled arrow heads) and delamination near the articular surface (open arrow heads). Overall, the 1.2 mm rod created fissures with smaller open area postimpact ((b), arrows) compared to open fissures postimpact in the 0.8 mm rod group ((c), box). The variation in fissures between the two rod diameters suggested that local mechanics were important in the creation of fissures because the local impact mechanics are more distinct between the two scenarios than the bulk mechanics.

$$F(t) = k \cdot d_B(t) \tag{2}$$

Bulk strain rate as a function of time was calculated as the difference between subsequent time points using the following equation:

$$\dot{\varepsilon}(t) = \frac{\varepsilon(\text{t}) - \varepsilon(\text{t} - 1)}{\Delta t} \tag{3}$$

To calculate bulk force rate as a function of time ($\dot{F}(t)$), ε is replaced with F in Eq. (3).

The temporal peak of each bulk quantity was extracted for subsequent analysis. Fissured samples were only analyzed up to the fissure event to avoid artifact from material rupture.

Local Strain. To evaluate mechanics on the length scale of fissures and cartilage material heterogeneities, Green–Lagrange strain tensor fields were calculated during impact using verified digital image correlation (DIC) code for the same 11 samples that were analyzed in bulk [38,39]. DIC was performed using visual texture created by polystyrene microspheres to determine two-dimensional strain fields with 10 pixel grid spacing (45 μm resolution). Local deformations were large; thus, DIC was performed relative to the previous time point, rather than the initial ($t = 0$) image. Strain error was less than 5%, as evaluated using generated data with known deformation of the real visual texture.

Three strain invariants and their respective rates and gradients were calculated from Green–Lagrange strain tensors: first and second principal strains and maximum shear strain. First principal strain is the most tensile strain and was selected due to its proposed importance in collagen fiber/fibril failure [40,41]. In two dimensions, second principal strain is the most compressive strain and was evaluated for comparison against bulk compressive strain. Finally, maximum shear strain was evaluated because of its relationship to maximum shear stress, which is the primary mode under which ductile materials fail [42] and because it has previously been proposed as a damage predictor in cartilage [36,43]. Strain rates were evaluated because cartilage is poroelastic with strongly rate-dependent material and failure behavior [44–46]. Local strain rates were calculated using second-order Savitzky–Golay filtering with a five-point window. Spatial gradients have also been proposed as important for cartilage damage. In particular, contact pressure gradients distinguish between intact and damaged cartilage more effectively than either peak or average contact pressure [47]. The spatial gradient of each local strain metric was calculated using linear finite-element shape functions. The magnitude of the strain gradient was reported. For comparisons between fissured and intact groups, the spatiotemporal peak of each strain variable was utilized.

Logistic Regression for Predicting Damage. Predictive models of cartilage fissuring were developed by fitting experimental data from samples impacted with the 1.2 mm diameter rod to logistic regression models (Fig. 2(a)). Each logistic regression model fits binary outcome data with a continuous sigmoidal curve based on continuous predictors [43,48]. The logistic regression fits (Eq. (4)) provided an equation for probability of fissure, given a specific value for any predictor variable (x) [48]

$$p = \frac{1}{1 + e^{-\left(\frac{x - a}{b}\right)}} \tag{4}$$

In Eq. (4), a is the value of the predictor variable at 50% probability of fissure, b controls the transition width from low probability to high probability and the ratio of a to b controls the offset probability when the predictor variable is zero. The binary outcome was

fissure state: intact (zero) or fissured (one). The continuous predictors were the four bulk and nine local mechanical variables: bulk strain, bulk strain rate, bulk force, bulk force rate, local first principal strain, local second principal strain, local maximum shear strain, local first principal strain rate, local second principal strain rate, local maximum shear strain rate, local gradient of first principal strain, local gradient of second principal strain, and local gradient of maximum shear strain.

To develop predictions based on bulk mechanics, each sample impacted with the 1.2 mm diameter rod was noted as either fissured or intact (17 fissured and six intact samples, $n = 23$ data points). The four individual bulk mechanical variables were used individually as predictor variables.

To develop predictions based on local strain, data from a subset of six samples impacted with the 1.2 mm diameter rod were fit to logistic regression models (three fissured and three intact samples, $n = 615$ data points). The temporal peak from each grid point was used for local logistic regression analyses. A relatively small number of samples could be used since each sample provides a large number of data points, reducing experimental burden.

All fissures occurred in the most superficial 300 μm, thus analysis focused on this region. Many fissures closed postimpact, resulting in a fissure line that could lie between grid points. To account for this, strain grid points less than 45 μm (one grid spacing) from a fissure were marked as fissured data points. To ensure that nonfissured points were sufficiently far from the fissure, grid points at least 90 μm (two grid spacings) away from the fissure
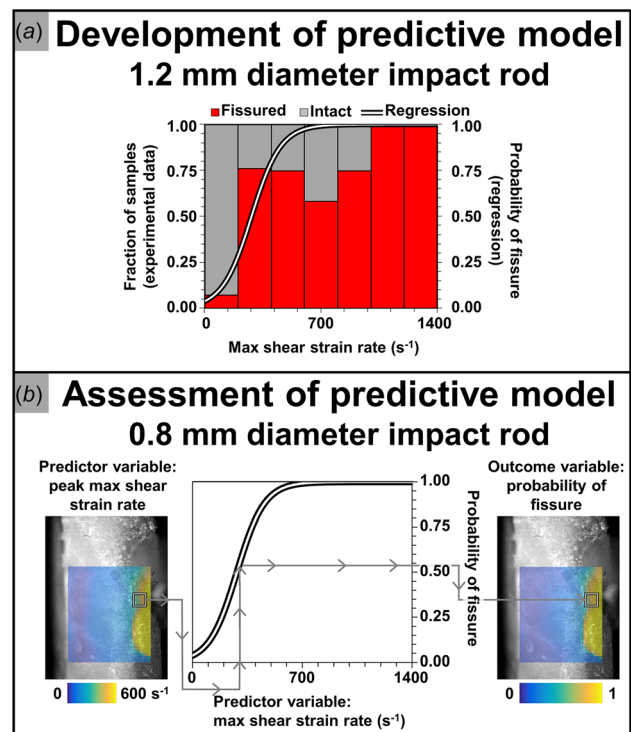

Fig. 2 Development and assessment of logistic regression models for predicting failure in cartilage. Models were developed using data from samples impacted with the 1.2 mm diameter rod (a). For local mechanics, the temporal peak of each mechanical variable was determined at each grid point. Regions near the articular surface that were fissured and intact were used to develop logistic regression models, providing multiple data points from each sample. For bulk mechanics, a single data point was used for each sample. Models were assessed using samples impacted with the 0.8 mm diameter rod (b). The predictor variable of interest (maximum shear strain rate in this example) was fed into the logistic regression model in order to yield the probability of fissure at each location on the sample.
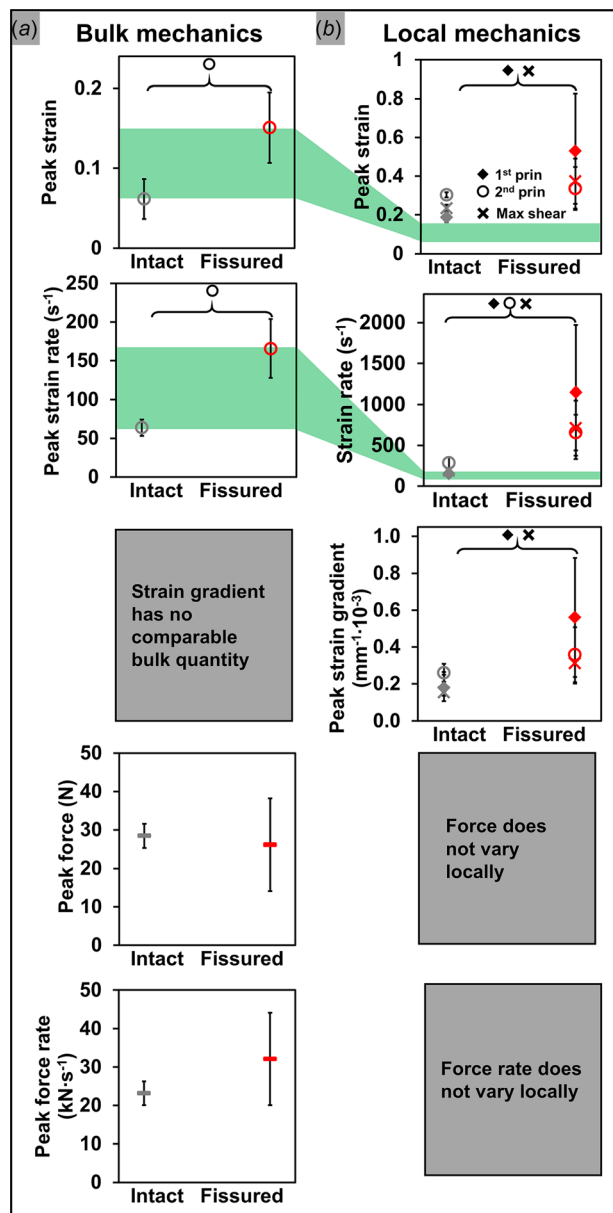
Fig. 3 In general, bulk (*a*) and local (*b*) mechanics were larger in fissured samples than in intact samples when averaged across impact energies in each group. Large differences in magnitude between bulk and local mechanics reflect heterogeneity in the local strain fields that is averaged out in bulk strain. These differences are highlighted by the shading, which shows the average bulk results for the intact and fissured samples on the local plots. Local peak strain and strain rate were about two and five times larger, respectively, than their bulk measures. In particular, peak local second principal strain (most compressive strain) was 3.5 ± 2.4 times larger than peak bulk strain (also compressive). Further, peak local second principal strain rate was 4.4 ± 1.8 times larger than peak bulk strain rate. Within bulk mechanics, strain and strain rate were significantly larger in fissured than intact samples, but there were no significant differences in force or force rate (*a*). Within local mechanics, first principal strain and maximum shear strain, all three strain rates, and the gradients of first principal strain and maximum shear strain were significantly larger in fissured than intact samples (*b*). In contrast to bulk results, wherein bulk strain is analogous to local second principal strain, local second principal strain was not significantly different between groups. Error bars = standard deviation. Symbol indicates $p \le 0.05$ for select variable.

were marked as intact data points. Each local strain metric was used as an individual predictor variable.

Assessment of Fissure Prediction. Predictive models of damage were evaluated using the 12 samples impacted with the 0.8 mm diameter rod (nine intact, three fissured). For bulk mechanics, a single prediction (fissured or intact) was made on each sample (12 data points). Additionally, data from all 12 samples were averaged to obtain cohort predictions using bulk mechanics. For local strain, sample-specific, spatially variant predictions were made on a subset of six samples from the 0.8 mm diameter rod cohort (three intact, three fissured; 582 data points total). Local strain fields were computed using DIC and then used to predict the probability of fissure for each sample at each strain grid point, producing a probability-of-fissure field (Fig. 2(*b*)). Comparisons were made between predicted and actual fissure.

Statistical Analysis. Differences between fissured and intact samples were tested using two-tailed, unequal variance t-tests. Logistic regression was completed using Stata, with significance tested using a two-tailed t-test versus the null hypothesis of each coefficient being zero (StataCorp LP, College Station, TX). All *p*-values were corrected with Finner's step down procedure [49]; corrected values are reported. Receiver operating characteristics (ROCs) curves were obtained by determining true and false positives at all fissure probabilities, from 0.001 to 1.000 in 0.001 increments. The area under the ROC curve, which is the concordance statistic (*c*-statistic) for binary data [50], was calculated using a Riemann sum.

Results

Bulk Strain and Force. A series of 11 samples impacted with the 1.2 mm diameter rod were used to compare mechanics between fissured and intact samples (seven fissured and four intact samples). Videos of sample deformation were analyzed, excluding frames after fissure occurred, and mechanical results were pooled across impact energies. Peak bulk strain and strain rate were significantly larger in fissured samples than in intact samples (Fig. 3(*a*)). On average, strain in fissured samples was 2.5 times larger than in intact samples, while strain rate was 2.6 times larger. There were no significant differences in force or force rate between the two groups (Fig. 3(*a*)). These differences in strain with consistent force suggest nonlinear material behavior prior to fissure.

Local Strain. Local strains were compared for the same samples used to compare bulk mechanics. Spatiotemporal peaks of all local strain variables, with the notable exceptions of second principal strain and gradient of second principal strain, were larger in fissured than in intact samples (Fig. 3(*b*)). On average, first principal strain was 2.8 times larger and maximum shear strain was 1.6 times larger in fissured than intact samples. First principal strain rate, second principal strain rate, and maximum shear strain rate were 2.3–7.6 times larger in fissured than in intact samples. The gradient of first principal strain and the gradient of maximum shear strain were 3.1 and 2.0 times larger in fissured than in intact samples, respectively. In contrast to bulk mechanics, where compressive strain was larger in fissured than in intact samples, there was no significant difference in local second principal strain between the two groups. Similarly, there was no significant difference in the gradient of second principal strain between the two groups.

Local strain patterns in both intact and fissured samples were highly heterogeneous (Fig. 4 and Supplemental Figs. S1–S9 are available under the "Supplemental Materials" tab for this paper on the ASME Digital Collection). In both cases, peak values were localized in a relatively shallow zone under the impact location. The ratio of peak local second principal strain to peak bulk
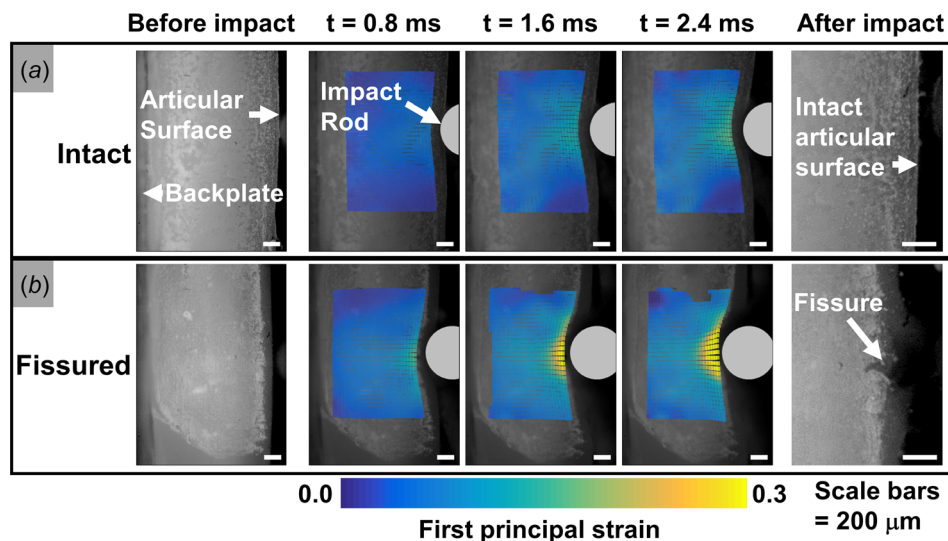
Fig. 4 First principal strain for a subset of time points during impact in representative intact (*a*) and fissured (*b*) samples. In both samples, large strains were concentrated under the impact location in the most superficial 500 μm of the sample (rod shaded for clarity). Peak magnitudes were larger in the fissured sample than in the intact sample. Following impact, the intact sample had an unchanged articular surface relative to the image before impact, while a fissure was visible in the fissured sample.

compressive strain was 3.5 ± 2.4, and the ratio of peak local second principal strain rate to peak bulk strain rate was 4.4 ± 1.8. Both of these ratios reflect heterogeneity in the local strain fields that is inherently averaged out in bulk strain measures.

Logistic Regression for Predicting Damage. Logistic regression fits (Fig. 2(*a*)) were statistically significant for all local predictor variables (three intact and three fissured samples, totaling 615 data points). Logistic regression fits approached statistical significance for all bulk predictors ($0.05 < p < 0.20$) (17 fissured and six intact samples). Having only a single data point for each sample resulted in fewer measurements overall and thus less statistical power for bulk variables than for local variables. Coefficients for each predictor variable, which can be used to predict probability of fissure using Eq. (4), are provided in Table 1.

Assessment of Fissure Prediction. Bulk mechanics were accurate predictors of fissure for the entire sample cohort, but poor predictors of fissure for individual samples (12 samples total, nine fissured, and three intact) (Fig. 5). For example, bulk strain predicted the probability of fissure as low as 0.10 in fissured samples and as high as 0.90 for intact samples. However, when bulk strain was averaged across all 12 samples and used to predict the

probability of fissure for the entire cohort, the prediction was 0.68, less than 10% different than the actual fissure rate of 0.75.

Local strain and strain rate predictions discriminated well between fissured and intact locations on impacted samples, with all *c*-statistics ≥ 0.75, when evaluated across six samples (three fissured and three intact samples, totaling 582 data points) (Fig. 6). Conversely, all *c*-statistics were less than 0.75 for strain gradient measures. First principal strain rate had the largest *c*-statistic (0.86), with a 0.50 fissure threshold of $324\,\text{s}^{-1}$. Gradient of second principal strain had the smallest *c*-statistic (0.68). Qualitatively, local strain predicted spatially heterogeneous patterns of fissure (Supplemental Fig. S10 is available under the "Supplemental Materials" tab for this paper on the ASME Digital Collection), with the quality of these predicted fissure patterns reflected in the quantitative *c*-statistic.

Discussion

Bulk Versus Local Mechanics. The first objective of this study was to quantify bulk and local mechanics in cartilage; this quantification demonstrated differences between the two length scales in both magnitude and trend. Bulk strain under-reported local peak compressive strain and strain rate by a factor of $\sim$3–4. This highlights the fact that bulk measures inherently average

Table 1 Regression coefficients for bulk and local predictors (95% confidence interval) to use with Eq. (4)

Predictor (x)	50% threshold (a)	Transition width (b)
Bulk compressive strain	$-0.0946\ (-0.220, -0.0303)$	$-0.0153\ (-0.00164, -0.0290)$
Bulk compressive strain rate (s^{-1})	$-102\ (-230, 269)\ \text{s}^{-1}$	$-26.2\ (-47.3, -5.09)\ \text{s}^{-1}$
Bulk force (N)	$14.2\ (-33.5, 62.1)\ \text{N}$	$15.1\ (-6.50, 36.7)\ \text{N}$
Bulk force rate (kN s^{-1})	$22.0\ (-15.2, 59.2)\ \text{kN·s}^{-1}$	$8.29\ (-0.0975, 16.7)\ \text{kN·s}^{-1}$
Local first principal strain	$0.165\ (0.128, 0.203)$	$0.0390\ (0.0324, 0.0456)$
Local second principal strain	$-0.237\ (-0.326, -0.149)$	$-0.156\ (-0.205, -0.108)$
Local maximum shear strain	$0.170\ (0.131, 0.209)$	$0.0500\ (0.0411, 0.0587)$
Local first principal strain rate (s^{-1})	$324\ (250, 398)\ \text{s}^{-1}$	$115\ (94.7, 136)\ \text{s}^{-1}$
Local second principal strain rate (s^{-1})	$-309\ (-397, -220)\ \text{s}^{-1}$	$-115\ (-143, -87)\ \text{s}^{-1}$
Local maximum shear strain rate (s^{-1})	$283\ (222, 344)\ \text{s}^{-1}$	$87.8\ (73.6, 102.1)\ \text{s}^{-1}$
Local grad of first principal strain (μm^{-1})	$1.77\ (1.27, 2.27) \times 10^{-4}\ \mu\text{m}^{-1}$	$5.41\ (4.20, 6.62) \times 10^{-5}\ \mu\text{m}^{-1}$
Local grad of second principal strain (μm^{-1})	$1.24\ (0.851, 1.64) \times 10^{-4}\ \mu\text{m}^{-1}$	$4.92\ (3.70, 6.14) \times 10^{-5}\ \mu\text{m}^{-1}$
Local grad of maximum shear strain (μm^{-1})	$1.33\ (0.982, 1.69) \times 10^{-4}\ \mu\text{m}^{-1}$	$4.77\ (3.80, 5.74) \times 10^{-5}\ \mu\text{m}^{-1}$

local data, smoothing spatial heterogeneities in the strain field. Because strain field heterogeneities correspond spatially with local damage phenomena such as fissuring, this smoothing hides relevant information. Further, the overall bulk strain needed to cause fissure varies between samples and studies (e.g., due to sample thickness), whereas local strain can be expected to remain more consistent. Interestingly, the local strain that is conceptually most similar to the bulk strain, namely the second principal strain, was not statistically different between groups. This discrepancy suggests that bulk compressive strain is a proxy for other local strain variables, which cannot be evaluated effectively in the bulk paradigm.

Predictive Models. The second objective of this study was to develop predictive models of fissuring based on bulk and local mechanics. Logistic regression fits were used to achieve this objective. While this idea is consistent with the ability of previous studies to fit logistic regression models to experimental data with continuous mechanical predictor variables [36,43], the data presented here include the first experimentally measured local mechanics to provide these fits.

Prediction Assessment. The third objective was to evaluate the accuracy of logistic regression models in predicting fissures in a second set of samples impacted with a different size rod. This tested the utility of local and bulk mechanics in predicting damage across loading conditions. The best local predictor was first principal strain rate, which suggests that the poroelastic nature of cartilage is important in the occurrence of fissures, in agreement with previous literature [44]. Further, principal strain as a failure criterion is consistent with brittle failure in collagen fibrils [51,52], and with previous observation of brittle failure in impact-induced cartilage injury as a result of high strain rates [30,53]. The second best local predictor was maximum shear strain. Maximum shear

Fig. 5 Predictions of fissures from bulk mechanics. For individual samples, many of the predictions were inaccurate, including predictions of high probability of fissure for intact samples and low probability of fissure for fissured samples. Conversely, cohort average predictions were accurate for the entire cohort as can be seen by comparing with the experimentally observed fissure rate (dashed line). Cohort average predictions were calculated by averaging each predictor for the cohort, and then predicting the probability of fissure from the average value. For example, bulk force data were first averaged across all 12 intact and fissured samples. This average force was then used as input to the regression model (Eq. (4)), which resulted in the cohort average prediction. Error bars were calculated from the average of each predictor for the cohort plus or minus one standard deviation. Predictions were developed using data from samples impacted with the 1.2 mm diameter rod and evaluated on data from samples impacted with the 0.8 mm diameter rod. (For color in this figure legend, the reader is referred to the web version of this article.)

stress is the primary failure mode in ductile materials [42], potentially indicating a ductile failure mechanism in cartilage. Maximum shear stress has also been previously proposed as an accurate predictor of cartilage fissuring [36,43]. Microscopic imaging of fissures can provide additional insight into potential failure mechanisms: visualization using scanning electron microscopy demonstrated visual features consistent with wedging followed by fibrillation and brittle failure with ductile pulling of fibers (Supplemental Fig. S11 is available under the "Supplemental Materials" tab for this paper on the ASME Digital Collection). These mechanisms are also seen in failure of polyethylene and polypropylene [54].

While bulk mechanics were poor predictors of failure on individual samples, they predicted the cohort-average failure rate well. This suggests that the selection of bulk or local mechanics for predicting damage is dependent upon the intended use of the resulting prediction. The selection of bulk mechanics is further dependent on the match between boundary and loading conditions used in developing predictive models, and boundary and loading conditions in the intended use of the predictions. For subject- or location-specific predictions, local mechanics would be preferred, as this would provide a link between macrolevel mechanics (e.g., those predicted using subject-specific finite-element analysis) and local, microlevel cartilage failure. However, for population-averaged predictions, bulk mechanics would be appropriate if the boundary and loading conditions are sufficiently similar to those used in developing predictive models.

Biological Implications. Although the present study did not evaluate the cellular response to impact, cell death is likely an important aspect in initiation of PTOA. In subfissure impact, chondrocyte death is concentrated near the articular surface [15,37]; in impact-induced fissuring, chondrocyte death is focused near fissures [55–57]. Thresholds for fissures are larger than for cell death, as can be demonstrated by comparison to previously measured local strain and cell death in subfissure impact [37]. Parallel to the articular surface, ∼9% tensile strain produced ∼50% probability of cell death, but only produced 12% probability of fissure. Perpendicular to the articular surface, ∼10% compressive strain produced ∼50% probability of cell death, but only produced 29% probability of fissure. In terms of progression of PTOA, the relative importance of chondrocyte death and structural damage are unknown, but it is likely that both act synergistically in the initiation and progression of cartilage degradation [58,59].

Considerations. Values and thresholds presented in this study should be compared with previously published data on bulk mechanics with caution since bulk mechanics are sensitive to sample geometry, boundary conditions, and loading conditions. Additionally, most previous studies have tested groups at discrete levels (e.g., two discrete peak stresses), thus an exact threshold cannot be determined. In adult human cartilage, the compressive strain at failure was 20–30% at strain rates of $1000 \, s^{-1}$ and $500 \, s^{-1}$ [27]. In the current study, a local compressive strain of 24% corresponded to 50% probability of fissure, which is consistent with the threshold in human cartilage. However, in this study, the threshold in bulk compressive strain was dramatically lower, with the 95% probability of fissure at 14% bulk compressive strain. This discrepancy may be due to differences in tissue source and boundary conditions, and thus underscores the value of evaluating local strain fields to circumvent interstudy variation.

Tissue source, boundary conditions, loading history, and the focus on strain rather than stress are all considerations in interpreting these data. The tissue source in this study was immature bovine. While there are concerns regarding the applicability of immature bovine tissue, there is evidence that its material behavior is qualitatively consistent with mature tissue, and with tissue from other species [60]. Therefore, the trends found here could be expected to be qualitatively similar in mature human tissue but
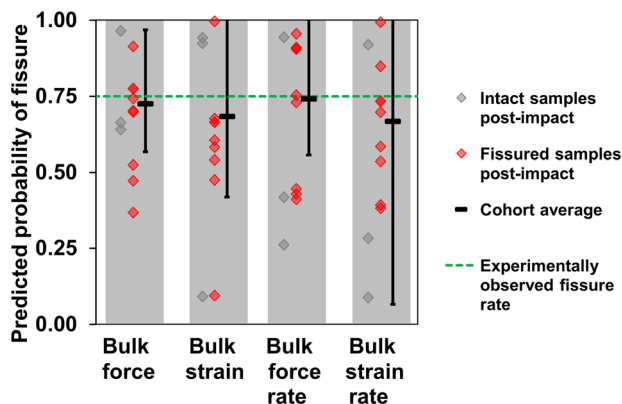
with different threshold parameters such that the present results cannot be directly translated to mature human cartilage. While the boundary and loading conditions used in this study do not replicate a loading environment seen in vivo, local mechanics provides information that is relatively independent of boundary and loading conditions. The insensitivity of local mechanics to sample boundary and loading conditions is actually one of the strengths of using local mechanics for failure prediction. Conversely, the bulk mechanics evaluated in this study are limited to this particular loading scenario. Similarly, sectioning cartilage to approximately 1 mm thick would be expected to affect bulk mechanics, but have a minimal effect on local mechanics, because they were evaluated far from that boundary. A previous study demonstrated the importance of the superficial zone to cartilage resilience to cellular injury under impact load [37]; thus, the intact articular surface enabled realistic failure thresholds in the present study. This study focused on strain and did not evaluate stress. The advantage of using strain is that it can be directly measured, while estimating or predicting stress in heterogeneous, nonlinear materials such as cartilage requires detailed information about the spatial variation of material properties. However, because stress is important in the failure of many materials, extensions of this research should include the evaluation of stresses for their ability to predict fissures. Finally, temporal and spatial peak values were selected for analysis. While maximum values are inherently less stable than mean values, the data in this study were relatively smooth (Fig. 1). Further, failure would be expected to occur at peak values, thus making them appropriate for establishing failure thresholds.
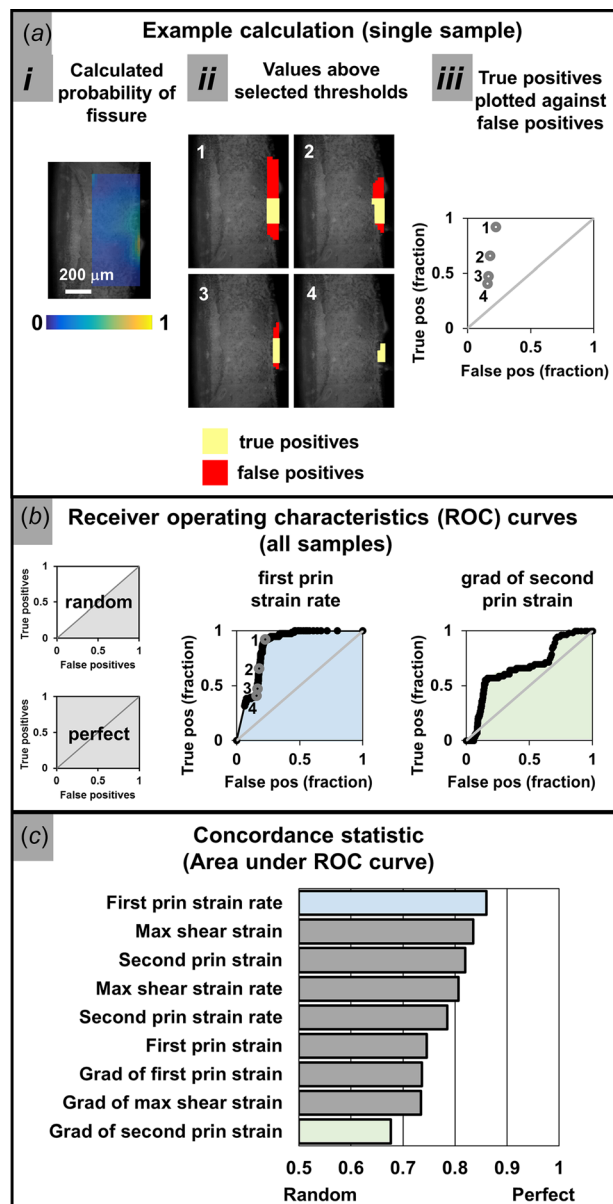
Conclusions. Overall, this study provides the first quantification of local strain fields during impact-induced fissuring. Further, this study demonstrates the ability of local strain to predict fissures, an important step in the goal of establishing causal links between mechanics and cartilage damage. In particular, these data suggest that rate-dependent phenomena are important in cartilage failure, and cartilage failure exhibits ductile and brittle features. These techniques can be expanded to include other failure criteria, and can be applied to other biological tissues. Ultimately, these data and other data collected using this framework can be used to link finite element-predicted mechanics to local tissue failure, and thereby accurately predict mechanically mediated diseases on a patient-specific basis.

Fig. 6 Concordance statistics (*c*-statistics) for local predictors. Grid points near the articular surface were analyzed (*a*): for each predictor variable, the probability of fissure was calculated (*i*). Grid points above a probability threshold were selected and categorized as either true positives (locations that did fissure) or false positives (locations that did not fissure) (*ii*). Normalized true positives were plotted against normalized false positives for all samples (*iii*). Steps (*ii*) and (*iii*) were repeated for all probabilities from 0.001 to 1.000 in increments of 0.001. The result from this process was the ROC curve for each predictor variable (*b*). The area under the ROC curve was calculated using a Riemann sum. The area under the curve is the *c*-statistic, and was compared between predictor variables (*c*). Strain and strain rate *c*-statistics were all ≥0.75, while strain gradient *c*-statistics were all <0.75. The maximum *c*-statistic was for first principal strain rate, while the minimum was for the gradient of second principal strain.

References

[1] Buckwalter, J. A., Anderson, D. D., Brown, T. D., Tochigi, Y., and Martin, J. A., 2013, "The Roles of Mechanical Stresses in the Pathogenesis of Osteoarthritis: Implications for Treatment of Joint Injuries," Cartilage, **4**(4), pp. 286–294.

[2] Kim, H. T., Lo, M. Y., and Pillarisetty, R., 2002, "Chondrocyte Apoptosis Following Intraarticular Fracture in Humans," Osteoarthritis Cartilage, **10**(9), pp. 747–749.

[3] Jeffrey, J. E., Gregory, D. W., and Aspden, R. M., 1995, "Matrix Damage and Chondrocyte Viability Following a Single Impact Load on Articular Cartilage," Arch. Biochem. Biophys., **322**(1), pp. 87–96.

[4] Kerin, A. J., Coleman, A., Wisnom, M. R., and Adams, M. A., 2003, "Propagation of Surface Fissures in Articular Cartilage in Response to Cyclic Loading In Vitro," Clin. Biomech., **18**(10), pp. 960–968.

[5] Aspden, R., 2002, "Letter to the Editor," Osteoarthritis Cartilage, **10**(7), pp. 588–589.

[6] Silverberg, J. L., Dillavou, S., Bonassar, L. J., and Cohen, I., 2013, "Anatomic Variation of Depth-Dependent Mechanical Properties in Neonatal Bovine Articular Cartilage," J. Orthop. Res., **31**(5), pp. 686–691.

[7] Buckley, M. R., Gleghorn, J. P., Bonassar, L. J., and Cohen, I., 2008, "Mapping the Depth Dependence of Shear Properties in Articular Cartilage," J. Biomech., **41**(11), pp. 2430–2437.

[8] Buckley, M. R., Bonassar, L. J., and Cohen, I., 2013, "Localization of Viscous Behavior and Shear Energy Dissipation in Articular Cartilage Under Dynamic Shear Loading," ASME J. Biomech. Eng., **135**(3), p. 31002.

[9] Chen, A. C., Bae, W. C., Schinagl, R. M., and Sah, R. L., 2001, "Depth- and Strain- Dependent Mechanical and Electromechanical Properties of Full-Thickness Bovine Articular Cartilage in Confined Compression," J. Biomech., **34**(1), pp. 1–12.

[10] Chen, S. S., Falcovitz, Y. H., Schneiderman, R., Maroudas, A., and Sah, R., 2001, "Depth-Dependent Compressive Properties of Normal Aged Human Femoral Head Articular Cartilage: Relationship to Fixed Charge Density," Osteoarthritis Cartilage, **9**(6), pp. 561–569.

[11] Backus, J. D., Furman, B. D., Swimmer, T., Kent, C. L., Mcnulty, A. L., Defrate, L. E., Guilak, F., and Olson, S. A., 2012, "Cartilage Viability and Catabolism in the Intact Porcine Knee Following Transarticular Impact Loading With and Without Articular Fracture," J. Orthop. Res., 29(4), pp. 501–510.

[12] Bolam, C. J., Hurtig, M. B., Cruz, A., and McEwen, B. J. E., 2006, "Characterization of Experimentally Induced Post-Traumatic Osteoarthritis in the Medial Femorotibial Joint of Horses," Am. J. Vet. Res., 67(3), pp. 433–447.

[13] Heiner, A. D., Smith, A. D., Goetz, J. E., Goreham-Voss, C. M., Judd, K. T., McKinley, T. O., and Martin, J. A., 2013, "Cartilage-on-Cartilage Versus Metal-on-Cartilage Impact Characteristics and Responses," J. Orthop. Res., 31(6), pp. 887–893.

[14] Milentijevic, D., and Torzilli, P. A., 2005, "Influence of Stress Rate on Water Loss, Matrix Deformation and Chondrocyte Viability in Impacted Articular Cartilage," J. Biomech., 38(3), pp. 493–502.

[15] Milentijevic, D., Helfet, D. L., and Torzilli, P. A., 2003, "Influence of Stress Magnitude on Water Loss and Chondrocyte Viability in Impacted Articular Cartilage," ASME J. Biomech. Eng., 125(5), p. 594.

[16] Torzilli, P. A., Grigiene, R., Borrelli, J., and Helfet, D. L., 1999, "Effect of Impact Load on Articular Cartilage: Cell Metabolism and Viability, and Matrix Water Content," ASME J. Biomech. Eng., 121(5), pp. 433–441.

[17] Borrelli, J., Tinsley, K., Ricci, W. M., Burns, M., Karl, I. E., and Hotchkiss, R., 2003, "Induction of Chondrocyte Apoptosis Following Impact Load," J. Orthop. Trauma, 17(9), pp. 635–641.

[18] Borrelli, J., Zhu, Y., Burns, M., Sandell, L., and Silva, M. J., 2004, "Cartilage Tolerates Single Impact Loads of as Much as Half the Joint Fracture Threshold," Clin. Orthop. Relat. Res., 426, pp. 266–273.

[19] Borrelli, J., Silva, M. J., Zaegel, M. A., Franz, C., and Sandell, L. J., 2009, "Single High-Energy Impact Load Causes Posttraumatic OA in Young Rabbits Via a Decrease in Cellular Metabolism," J. Orthop. Res., 27(3), pp. 347–352.

[20] Borrelli, J., Zaegel, M. A., Martinez, M. D., and Silva, M. J., 2010, "Diminished Cartilage Creep Properties and Increased Trabecular Bone Density Following a Single, Sub-Fracture Impact of the Rabbit Femoral Condyle," J. Orthop. Res., 28(10), pp. 1307–1314.

[21] Ewers, B. J., Newberry, W. N., and Haut, R. C., 2000, "Chronic Softening of Cartilage Without Thickening of Underlying Bone in a Joint Trauma Model," J. Biomech., 33(12), pp. 1689–1694.

[22] Newberry, W. N., Garcia, J. J., Mackenzie, C. D., Decamp, D. E., and Haut, R. C., 1998, "Analysis of Acute Mechanical Insult in an Animal Model of Post-Traumatic Osteoarthritis," ASME J. Biomech. Eng., 120(12), pp. 704–709.

[23] Haut, R., Ide, T., and De Camp, C., 1995, "Mechanical Responses of the Rabbit Patello-Femoral Joint to Blunt Impact," ASME J. Biomech. Eng., 117(11), pp. 402–408.

[24] Ewers, B. J., Jayaraman, V. M., Banglmaier, R. F., and Haut, R. C., 2002, "Rate of Blunt Impact Loading Affects Changes in Retropatellar Cartilage and Underlying Bone in the Rabbit Patella," J. Biomech., 35(6), pp. 747–755.

[25] Burgin, L. V., and Aspden, R. M., 2008, "Impact Testing to Determine the Mechanical Properties of Articular Cartilage in Isolation and on Bone," J. Mater. Sci.: Mater. Med., 19(2), pp. 703–711.

[26] Lee, C. M., Kisiday, J. D., McIlwraith, C. W., Grodzinsky, A. J., and Frisbie, D. D., 2013, "Development of an In Vitro Model of Injury-Induced Osteoarthritis in Cartilage Explants From Compressive Overload," Am. J. Vet. Res., 74(1), pp. 40–47.

[27] Repo, R., and Finlay, J., 1977, "Survival of Articular Cartilage After Controlled Impact," J. Bone Jt. Surg., Am., 59(8), pp. 1068–1076.

[28] Patwari, P., Cheng, D. M., Cole, A. A., Kuettner, K. E., and Grodzinsky, A. J., 2007, "Analysis of the Relationship Between Peak Stress and Proteoglycan Loss Following Injurious Compression of Human Post-Mortem Knee and Ankle Cartilage," Biomech. Model. Mechanobiol., 6(1–2), pp. 83–89.

[29] Kim, W., Thambyah, A., and Broom, N., 2012, "Does Prior Sustained Compression Make Cartilage-on-Bone More Vulnerable to Trauma?," Clin. Biomech. (Bristol, Avon), 27(7), pp. 637–645.

[30] Thambyah, A., Shim, V. P. W., Chong, L. M., and Lee, V. S., 2008, "Impact-Induced Osteochondral Fracture in the Tibial Plateau," J. Biomech., 41(6), pp. 1236–1242.

[31] Ewers, B. J., Weaver, B. T., and Haut, R. C., 2002, "Impact Orientation Can Significantly Affect the Outcome of a Blunt Impact to the Rabbit Patellofemoral Joint," J. Biomech., 35(12), pp. 1591–1598.

[32] Leucht, F., Dürselen, L., Hogrefe, C., Joos, H., Reichel, H., Schmitt, H., Ignatius, A., and Brenner, R. E., 2012, "Development of a New Biomechanically Defined Single Impact Rabbit Cartilage Trauma Model for In Vivo-Studies," J. Invest. Surg., 25(4), pp. 235–241.

[33] Natoli, R. M., Scott, C. C., and Athanasiou, K. A., 2008, "Temporal Effects of Impact on Articular Cartilage Cell Death, Gene Expression, Matrix Biochemistry, and Biomechanics," Ann. Biomed. Eng., 36(5), pp. 780–792.

[34] Verteramo, A., and Seedhom, B. B., 2007, "Effect of a Single Impact Loading on the Structure and Mechanical Properties of Articular Cartilage," J. Biomech., 40(16), pp. 3580–3589.

[35] Patwari, P., Cheng, D. M., Cole, A. A., Kuettner, K. E., and Grodzinsky, A. J., 2007, "Analysis of the Relationship Between Peak Stress and Proteoglycan Loss Following Injurious Compression of Human Post-Mortem Knee and Ankle Cartilage," Biomech. Model. Mechanobiol., 6(1–2), pp. 83–89.

[36] Atkinson, T., Haut, R., and Altiero, N., 1998, "Impact-Induced Fissuring of Articular Cartilage: An Investigation of Failure Criteria," ASME J. Biomech. Eng., 120(2), pp. 181–187.

[37] Bartell, L. R., Fortier, L. A., Bonassar, L. J., and Cohen, I., 2015, "Measuring Microscale Strain Fields in Articular Cartilage During Rapid Impact Reveals Thresholds for Chondrocyte Death and a Protective Role for the Superficial Layer," J. Biomech., 48(12), pp. 3440–3446.

[38] Jones, E. M. C., Silberstein, M. N., White, S. R., and Sottos, N. R., 2014, "In Situ Measurements of Strains in Composite Battery Electrodes During Electrochemical Cycling," Exp. Mech., 54(6), pp. 971–985.

[39] Jones, E. M. C., 2013, "Improved Digital Image Correlation," MatLab Central, Natick, MA, Aug. 14, accessed Dec. 14, 2014, http://www.mathworks.com/matlabcentral/fileexchange/43073-improved-digital-image-correlation–dic-

[40] Kafka, V., 2002, "Surface Fissures in Articular Cartilage: New Concepts, Hypotheses and Modeling," Clin. Biomech., 17(1), pp. 73–80.

[41] Hadi, M. F., Sander, E. A., and Barocas, V. H., 2012, "Multiscale Model Predicts Tissue-Level Failure From Collagen Fiber-Level Damage," ASME J. Biomech. Eng., 134(9), pp. 091005–091005-10.

[42] Beer, F. P., Johnston, E. R., Jr., DeWolf, J. T., and Mazurek, D. F., 2012, Mechanics of Materials, McGraw-Hill Education, New York.

[43] Atkinson, T., Haut, R., and Altiero, N., 1998, "An Investigation of Biphasic Failure Criteria for Impact-Induced Fissuring of Articular Cartilage," ASME J. Biomech. Eng., 120(4), pp. 536–537.

[44] Morel, V., and Quinn, T. M., 2004, "Cartilage Injury by Ramp Compression Near the Gel Diffusion Rate," J. Orthop. Res., 22(1), pp. 145–151.

[45] Mow, V. C., Kuei, S. C., Lai, W. M., and Armstrong, C. G., 1980, "Biphasic Creep and Stress Relaxation of Articular Cartilage in Compression: Theory and Experiments," ASME J. Biomech. Eng., 102(1), pp. 73–84.

[46] Huang, C.-Y., Soltz, M. A., Kopacz, M., Mow, V. C., and Ateshian, G. A., 2003, "Experimental Verification of the Roles of Intrinsic Matrix Viscoelasticity and Tension-Compression Nonlinearity in the Biphasic Response of Cartilage," ASME J. Biomech. Eng., 125(1), pp. 84–93.

[47] Brand, R. A., 2005, "Joint Contact Stress: A Reasonable Surrogate for Biological Processes?," Iowa Orthop. J., 25, pp. 82–94.

[48] Hosmer, D. W., and Lemeshow, S., 2000, Applied Logistic Regression, Wiley, Hoboken, NJ.

[49] Finner, H., 1993, "On a Monotonicity Problem in Step-Down Multiple Test Procedures," J. Am. Stat. Assoc., 88(423), pp. 920–923.

[50] Steyerberg, E. W., Vickers, A. J., Cook, N. R., Gerds, T., Obuchowski, N., Pencina, M. J., and Kattan, M. W., 2010, "Assessing the Performance of Prediction Models: A Framework for Some Traditional and Novel Measures," Epidemiology, 21(1), pp. 128–138.

[51] Tang, Y., Ballarini, R., Buehler, M. J., and Eppell, S. J., 2010, "Deformation Micromechanisms of Collagen Fibrils Under Uniaxial Tension," J. R. Soc., Interface, 7(46), pp. 839–850.

[52] Shen, Z. L., Dodge, M. R., Kahn, H., Ballarini, R., and Eppell, S. J., 2010, "in vitro Fracture Testing of Submicron Diameter Collagen Fibril Specimens," Biophys. J., 99(6), pp. 1986–1995.

[53] Silyn-Roberts, H., and Broom, N. D., 1990, "Fracture Behavior of Cartilage-on-Bone in Response to Repeated Impact Loading," Connect. Tissue Res., 24(2), pp. 143–156.

[54] Dasari, A., and Misra, R. D. K., 2003, "On the Strain Rate Sensitivity of High Density Polyethylene and Polypropylenes," Mater. Sci. Eng.: A, 358(1–2), pp. 356–371.

[55] Novakofski, K. D., Williams, R. M., Fortier, L. A., Mohammed, H. O., Zipfel, W. R., and Bonassar, L. J., 2014, "Identification of Cartilage Injury Using Quantitative Multiphoton Microscopy," Osteoarthritis Cartilage, 22(2), pp. 355–362.

[56] Lewis, J. L., Deloria, L. B., Oyen-Tiesma, M., Thompson, R. C., Ericson, M., and Oegema, T. R., 2003, "Cell Death After Cartilage Impact Occurs Around Matrix Cracks," J. Orthop. Res., 21(5), pp. 881–887.

[57] Ewers, B. J., Dvoracek-Driksna, D., Orth, M. W., and Haut, R. C., 2001, "The Extent of Matrix Damage and Chondrocyte Death in Mechanically Traumatized Articular Cartilage Explants Depends on Rate of Loading," J. Orthop. Res., 19(5), pp. 779–784.

[58] Martin, J. A., Brown, T., Heiner, A., and Buckwalter, J. A., 2004, "Post-Traumatic Osteoarthritis: The Role of Accelerated Chondrocyte Senescence," Biorheology, 41(3–4), pp. 479–491.

[59] Mow, V. C., and Huiskes, R., 2005, Basic Orthopaedic Biomechanics and Mechano-Biology, Lippincott Williams & Wilkins, Philadelphia, PA.

[60] Buckley, M. R., Bergou, A. J., Fouchard, J., Bonassar, L. J., and Cohen, I., 2010, "High-Resolution Spatial Mapping of Shear Properties in Cartilage," J. Biomech., 43(4), pp. 796–800.